ATLAS-INDET-NOTE XXX
21 January 1998

Parameterisation of the Inner Detector Performance

Ernst-Jan Buis[1], Reinier Dankers[2], Armin Reichold[3]
NIKHEF, Amsterdam, Netherlands.

Stephen Haywood[4]
Rutherford Appleton Laboratory, Chilton, Didcot, United Kingdom.

Abstract

A parameterisation of the track parameter resolutions in the Inner Detector of ATLAS has been used to implement a set of FORTRAN subroutines that can smear charged particle tracks according to these resolutions. The correlations between the track parameters have been taken into account. The data describing the detector performance has been intensively tested for self consistency and compared with results from the Inner Detector TDR.

[1] email r96@nikhef.nl
[2] email r78@nikhef.nl
[3] email a.reichold@nikhef.nl
[4] email s.haywood@rl.ac.uk

Table of contents

1 Introduction

For many ATLAS physics topics, a fast parametric detector simulation is needed. Until today many studies of SUGRA physics have been done with such simulations. So far, only a rudimentary description of the Inner Detector has been available for these studies. This work presents a complete parameterisation of the ATLAS Inner Detector. This parameterisation is implemented as a set of FORTRAN subroutines and functions and is currently used in ATLFAST [5]. From a given set of track parameters a smeared set of track parameters is calculated. The resolution used to calculate the smeared set is a good approximation to the current best estimate of the Inner Detector performance [1].

Smearing is done according to the particle type. The three particle types distinguished are electrons, muons and pions. All other charged particles are treated as pions. It is assumed that the smearing of each track parameter for muons and pions can be described by two uncorrelated parts - a Gaussian centre part and a tail. The Gaussian part is identical for muons and pions; the tails are different. For electrons, the smearing is more complicated. The division in an uncorrelated Gaussian part and a tail is probably not correct. Especially important are the low energy tails caused by Bremsstrahlung. At the moment only an accurate description of the central Gaussian part for muons and pions is available. More work is required to describe the tails and the electrons.

2 Track parameters

A track in the magnetic field of the Inner Detector can be described by a set of 5 parameters $\boldsymbol{p}$:

$$\boldsymbol{p} = \left(a_0, z_0, \phi_0, \cot\theta, Q/p_T \right) \tag{2.1}$$

These parameters are shown in figure 2.1 and figure 2.2.

Error! Not a valid link.

Figure 2.1 The track parameters in the *x*-*y* plane.

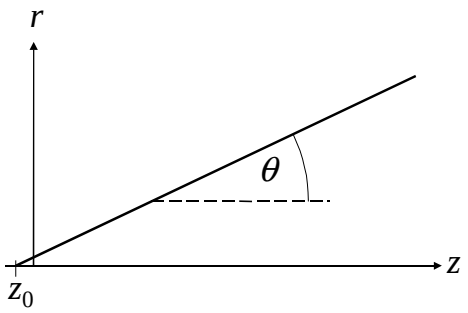

Figure 2.2 The track parameters in the *r*-*z* plane.

The transverse impact parameter a_0 is defined as the distance of closest approach to the beam-line. The sign of a_0 is negative if the track has positive angular momentum around the beam line. The longitudinal impact parameter z_0 is defined as the value of z at the point on the track where a_0 is evaluated. The angular co-ordinates are ϕ_0 and $\cot\theta$. Parameter ϕ_0 is the angle between the track and the x-axis at the point of closest approach. The inverse slope of the track in the r-z-plane is $\cot\theta$. The inverse transverse momentum Q/p_T, (Q = charge of the particle), and not p_T, is the quantity measured with Gaussian errors. The relation between R_{curv} and Q/p_T is given by:

$$R_{curv}[\mathrm{m}] = \frac{p_T[\mathrm{GeV}]}{0.3 \cdot Q[\mathrm{e}] \cdot B[\mathrm{T}]} \tag{2.2}$$

Because the errors on the 5 track parameters are not independent, they are described by a $5 \otimes 5$ covariance matrix $\boldsymbol{C}$. The diagonal elements are the squared sigma values $C_{aa} = \mathrm{cov}(p_a) = \sigma_a^2$. The off-diagonal terms are $C_{ab} = \mathrm{cov}(p_a, p_b) = \rho_{ab}\sigma_a\sigma_b$, with ρ_{ab} the correlation between parameter p_a and parameter p_b ($|\rho_{ab}| \leq 1$). Because in a very good approximation the variables in the *x*-*y* and *r*-*z* planes are independent, only 2*4 covariances are not zero; namely cov(Q/p_T, ϕ_0), cov(Q/p_T, a_0), cov(ϕ_0, a_0) and cov($\cot\theta$, z_0). Covariance matrices are always symmetric, invertible and positive definite[5].

If a beam constraint is used, an extra measurement is added with a value of 0 and a Gaussian error of 15 μm (beam radius). In this case a measurement of a_0 makes sense only when the resolution of a_0 without beam constraint is better than 15 μm. This is only true if a B-layer is used and if the track has a p_T of more than 20 GeV (section 4.1). Therefore no covariances including a_0 with beam constraint are given in this document.

3 Calculating covariance matrices

This chapter describes how the track parameter covariance matrices that are the input for the Inner Detector performance parameterisations are calculated.

A modified version of the Monte Carlo program `Presol` [4] has been used to calculate these covariance matrices. First a list of p_T and η values[6], representing the complete range of interest, has been defined. For each value of p_T and η one matrix has been calculated and stored. This matrix has been calculated as the weighted average[7] of approximately 50 matrices for different z_0, distributed according to a Gaussian profile around $z = 0$. The calculation of these matrices is described in more detail below.

3.1 Detector Model

The complete SCT tracker is implemented in the program `Presol`, including the pixel detector, and optionally including the B-layer. The TRT is also implemented. All subdetectors are modelled as continuous surfaces in a cylindrical geometry. The TRT is treated as 8 layers (both barrel and endcap), which is an approximation. All detector resolutions are based on full `DICE` simulation. The material is implemented in a simplified form. Local inhomogeneities are ignored. Both an ideal uniform 2T magnetic field and a more realistic solenoid field are available. One can optionally use a beam constraint. The agreement between the results from `Presol` and the results from full detector simulation is very good [1].

3.2 Derivation of covariance matrix

The measurements of the co-ordinates at which a track crosses a detector plane can be represented by a vector $\boldsymbol{h} = (t, z)$, with $t = r\phi$ (transverse co-ordinate). These measurements can be predicted as a function of r and the track parameter vector $\boldsymbol{p}$ (2.1). In a high-momentum approximation (the parabolic approximation of a circle is valid), the predicted co-ordinate vector $\hat{\boldsymbol{h}} = (\hat{t}, \hat{z})$ is given by[8] (homogenous field):

$$\begin{aligned} \hat{t}(r, \boldsymbol{p})[\mathrm{m}] &= a_0[\mathrm{m}] + \phi_0 r[\mathrm{m}] + 0.15B[\mathrm{T}]r^2[\mathrm{m}^2]\frac{Q[\mathrm{e}]}{p_T[\mathrm{GeV}]} \\ \hat{z}(r, \boldsymbol{p})[\mathrm{m}] &= z_0[\mathrm{m}] + \cot\theta r[\mathrm{m}] \end{aligned} \qquad (3.2.1)$$

---

[5] Positive definite means that for each vector $\boldsymbol{t}$: $\sum_{i=1}^{5}\sum_{j=1}^{5} C_{ij}t_i t_j > 0$.

[6] The p_T values vary between 0.5 GeV and 1 TeV. The $|\eta|$ values vary between 0 and 2.5. See also section 5.2.

[7] The best method is to calculate the average of the matrix coefficients. The original version of `Presol` (which produced the data in the TDR) calculated the average of the sigma values. Especially for $\eta = 0$, where results for different z_0 vary most, this can cause the final matrix to be non-positive definite.

[8] The expression for $\hat{z}$ in (3.2.1) is only valid for $|z - z_0| >> |a_0|$. Strictly z_0 in (3.2.1) is the intersection of the track with the *z*-axis. The interpretation of z_0 given in section 2 is only approximately valid.

For a solenoid magnetic field: $\vec{\boldsymbol{B}} = \vec{\boldsymbol{B}}(r, z)$. In this case (3.2.1) should be replace by [7]:

$$\begin{aligned} \hat{t}(r, \boldsymbol{p}) &= a_0 + \phi_0 r + 0.3\frac{Q}{p_T}\int_0^r\int_0^{r'}\left(B_z(r'', \hat{z}(r'', \boldsymbol{p})) - \cot\theta\, B_r(r'', \hat{z}(r'', \boldsymbol{p}))\right)dr'dr'' \\ \hat{z}(r, \boldsymbol{p}) &= z_0 + \cot\theta r \end{aligned} \tag{3.2.2}$$

Multiple scattering at the detector planes introduces additional parameters $\boldsymbol{p}_{ms}$, i.e. the two (fitted) deflections ($\Delta\phi$, $\Delta\cot\theta$) at each detection plane:

$$\boldsymbol{p}_{ms} = \left(\Delta\phi_0, \Delta\cot\theta_0, \Delta\phi_1, \Delta\cot\theta_1, \cdots, \Delta\phi_n, \Delta\cot\theta_n\right) \tag{3.2.3}$$

For n detection planes, $\boldsymbol{p}_{ms}$ has only $2n - 2$ (instead of $2n$) terms unequal to zero, because a measurement is only influenced by the multiple scattering that occurred in the material in front of the measurement. The scattering processes in the different planes are independent from each other. The multiple scattering angles, together with the helix parameters, give a full description of the path of a particle through the detector. The expected co-ordinate at plane i, $\hat{h}_i(r_i, \boldsymbol{p}, \boldsymbol{p}_{ms})$, is now given by:

$$\begin{aligned} \hat{t}_i(r_i, \boldsymbol{p}, \boldsymbol{p}_{ms}) &= a_0 + \phi_0 r_i + 0.3\frac{Q}{p_T}\int_0^r\int_0^{r'}\left(B_z(r'', \hat{z}(r'', \boldsymbol{p})) - \cot\theta\, B_r(r'', \hat{z}(r'', \boldsymbol{p}))\right)dr'dr'' + \sum_{j=1}^{i-1}\Delta\phi_j(r_i - r_j) \\ \hat{z}_i(r_i, \boldsymbol{p}, \boldsymbol{p}_{ms}) &= z_0 + \cot\theta r_i + \sum_{j=1}^{i-1}\Delta\cot\theta_j(r_i - r_j) \end{aligned} \tag{3.2.4}$$

The χ^2 for a fit of this prediction to the measurements can be split into a contribution from the intrinsic errors and a contribution from the multiple scattering terms:

$$\chi^2 = \chi^2_{in} + \chi^2_{ms} \tag{3.2.5}$$

For a set of n detection planes, the intrinsic part χ^2_{in} is given by:

$$\chi^2_{in} = \tfrac{1}{2}\sum_{i=1}^{n}\left(\boldsymbol{h}_i - \hat{\boldsymbol{h}}_i(r_i, \boldsymbol{p}, \boldsymbol{p}_{ms})\right)^{\mathrm{T}}\ \boldsymbol{R}_{ii}^{-1}\left(\boldsymbol{h}_i - \hat{\boldsymbol{h}}_i(r_i, \boldsymbol{p}, \boldsymbol{p}_{ms})\right) \tag{3.2.6}$$

The genuine error in the measurement of the position $\boldsymbol{h}_i$ at which the particle crossed plane number i is given through the plane's intrinsic resolutions and included in (3.2.6) through the term $\boldsymbol{R}_{ii}^{-1}$. This term is the inverse covariance matrix of $\boldsymbol{h}_i$. In our case $\boldsymbol{R}_{ii}$ has the following form[9]:

$$\boldsymbol{R}_{ii} = \begin{pmatrix} \sigma^2_{r\phi,i} & 0 \\ 0 & \sigma^2_{z,i} \end{pmatrix} \tag{3.2.7}$$

Both barrel and forward detectors do not necessarily measure $r\phi$ and z directly, but rather a longitudinal and transverse co-ordinate[10]. For the barrel strip detectors the relation between the detectors intrinsic resolutions at normal incidence (σ_L, σ_T) and the errors $(\sigma_{r\phi}, \sigma_z)$ is given as follows[11]:

$$\sigma_{r\phi} = \sigma_T \qquad \sigma_z = \sigma_L \tag{3.2.8}$$

For the barrel pixel detectors, this relation is given by:

$$\sigma_{r\phi} = \Omega\cdot\sigma_T \qquad \sigma_z = \frac{\sigma_L}{\sin\theta + \cos\theta} \tag{3.2.9}$$

---

[9] This is a diagonal matrix because the coupling of the two co-ordinates by the small stereo angle is neglected.

[10] The longitudinal co-ordinate is parallel to a strip or row of pixels, the transverse is perpendicular to it.

[11] A detailed list of the intrinsic errors used for this work can be found in the source code of `Presol`. In section 5 the location of the source code is given.

In the endcap area $r(z)$ and not $z(r)$ is measured. Therefore one finds (both for the pixel and strip detectors):

$$\sigma_{r\phi} = \sigma_T \qquad \sigma_z = \sigma_L \cot\theta \tag{3.2.10}$$

The term $(\sin\theta + \cos\theta)^{-1}$ in (3.2.9) describes the pixel resolution as function of θ. The resolution improves for increasing θ, caused by the increased cluster size. For bigger values of θ the resolution gets worse again, because the clusters become too big and break up. The best resolution is at 45°. The factor Ω is an $|\eta|$ dependant correction term, varying between 1 and 1.7 [4]. Both $(\sin\theta + \cos\theta)^{-1}$ and Ω are empirical terms to tune the resolution to full simulation.

For a set of $m = n - 1$ scattering planes, the multiple scattering term χ^2_{ms} is given by:

$$\chi^2_{ms} = \tfrac{1}{2}\sum_{i=1}^{m} \boldsymbol{p}^T_{i,ms} \boldsymbol{N}^{-1}_{ii} \boldsymbol{p}_{i,ms} \tag{3.2.11}$$

The vector $\boldsymbol{p}_{i,ms}$ is given by:

$$\boldsymbol{p}_{i,ms} = \left(\Delta\phi_i, \Delta\cot\theta_i\right) \tag{3.2.12}$$

The matrix $\boldsymbol{N}_{ii}$ describes the rms of the scattering angle at plane i:

$$\boldsymbol{N}_{ii} = \begin{pmatrix} \dfrac{k^2_{i,1}}{p^2_T} & 0 \\ 0 & \dfrac{k^2_{i,2}}{p^2_T} \end{pmatrix} \tag{3.2.13}$$

The terms $k_{i,1}$ and $k_{i,2}$ are given by:

$$k_{i,1} = 0.0136\sqrt{L_i[1+0.038\log L_i]^2 - L_{i-1}[1+0.038\log L_{i-1}]^2} \qquad k_{i,2} = \frac{k_{i,1}}{\sin\theta} \tag{3.2.14}$$

The term L_i describes the total radiation length, summed over all planes up to the current plane i:

$$L_i = \sum_{j=1}^{i} l_i \tag{3.2.15}$$

The term l_i describes the radiation length at plane i[12]. Equation (3.2.14)is an empirical extension of the formula given in [6], describing a single scattering. Equation (3.2.6) and (3.2.11) can be combined in one expression if the scattering angles at each detector plane are also regarded as measurements and are always zero. The measured position at plane i is now given by:

$$h_i = \left(t_i, z_i, 0, 0\right) \tag{3.2.16}$$

The predicted position $\hat{h}_i$ at plane i is given by:

$$\hat{h}_i = \left(\hat{t}_i(r, \boldsymbol{p}, \boldsymbol{p}_{ms}), \hat{z}_i(r, \boldsymbol{p}, \boldsymbol{p}_{ms}), \Delta\phi_i, \Delta\cot\theta_i\right) \tag{3.2.17}$$

The total error χ^2 is now given by:

$$\chi^2 = \tfrac{1}{2}\sum_{i=1}^{n} \left(\boldsymbol{h}_i - \hat{\boldsymbol{h}}_i(r_i, \boldsymbol{p}, \boldsymbol{p}_{ms})\right)^{\mathrm{T}} \boldsymbol{V}^{-1}_{ii} \left(\boldsymbol{h}_i - \hat{\boldsymbol{h}}_i(r_i, \boldsymbol{p}, \boldsymbol{p}_{ms})\right) \tag{3.2.18}$$

The 4 ⊗ 4 diagonal matrix $\boldsymbol{V}$ is given by:

$$\boldsymbol{V} = \begin{pmatrix} \boldsymbol{R} & \boldsymbol{0} \\ \boldsymbol{0} & \boldsymbol{N} \end{pmatrix} \tag{3.2.19}$$

---

[12] A detailed list of the radiation lengths for each plane can be found in the source code of `Presol`.

Having expressed the χ^2 in terms of $\boldsymbol{V}$, $\boldsymbol{h}$ and $\hat{\boldsymbol{h}}$ and knowing the functional dependence of $\hat{\boldsymbol{h}}$ from the track parameters $\boldsymbol{p}$ and multiple scattering parameters $\boldsymbol{p}_{ms}$, one can analytically determine the inverse covariance matrix $\boldsymbol{C}^{-1}$ of $\boldsymbol{p}$ and $\boldsymbol{p}_{ms}$:

$$\frac{\partial^2 \chi^2}{\partial \tilde{p}_a \partial \tilde{p}_b} = C_{ab}^{-1} = \sum_{i=1}^{n} \boldsymbol{D}_{i,a}^T \boldsymbol{V}_{ii}^{-1} \boldsymbol{D}_{i,b} \tag{3.2.20}$$

where:

$$\boldsymbol{D}_{i,a} = \frac{\partial \hat{\boldsymbol{h}}_i}{\partial \tilde{p}_a} \tag{3.2.21}$$

with $\tilde{\boldsymbol{p}}$ being the combined vector ($\boldsymbol{p}$, $\boldsymbol{p}_{ms}$).

Following from (3.2.4) one finds for each plane i the complete $(5 + 2n) \otimes 4$ matrix $\boldsymbol{D}_i$ to be:

$$\boldsymbol{D}_i = \begin{array}{c} \begin{array}{cccccccccccccc} \tilde{\boldsymbol{p}} \to a_0 & z_0 & \phi_0 & \cot\theta & {}^{Q}\!/_{p_T} & \Delta\phi_1 & \Delta\cot\theta_1 & \cdots & \Delta\phi_{i-1} & \Delta\cot\theta_{i-1} & \Delta\phi_i & \Delta\cot\theta_i & \Delta\phi_{i+1} & \cdots & \Delta\cot\theta_n \end{array} \\ \begin{pmatrix} 1 & 0 & r_i & 0 & 0.15 B_i r_i^2 & r_i - r_1 & 0 & \cdots & r_i - r_{i-1} & 0 & 0 & 0 & 0 & \cdots & 0 \\ 0 & 1 & 0 & r_i & 0 & 0 & r_i - r_1 & \cdots & 0 & r_i - r_{i-1} & 0 & 0 & 0 & \cdots & 0 \\ 0 & 0 & 0 & 0 & 0 & 0 & 0 & \cdots & 0 & 0 & 1 & 0 & 0 & \cdots & 0 \\ 0 & 0 & 0 & 0 & 0 & 0 & 0 & \cdots & 0 & 0 & 0 & 1 & 0 & \cdots & 0 \end{pmatrix} \end{array} \begin{array}{c} \hat{\boldsymbol{h}}_i \\ \downarrow \\ \hat{t}_i \\ \hat{z}_i \\ \Delta\phi_i \\ \Delta\cot\theta_i \end{array} \tag{3.2.22}$$

The term B_i describes the value of the magnetic field at the track intersection with the detector layer. In `Presol`, the $5 \otimes 5$ covariance matrices $\boldsymbol{C}$ as function of the original track parameters $\boldsymbol{p}$ only, are calculated by numerically inverting (3.2.20), after substituting (3.2.22) into it, and taking the $5 \otimes 5$ sub-matrix.

3.3 The $A \oplus B$ Model

The above formulas can be simplified if a measurement predominantly depends on the first two measurement planes. This is the case for the impact parameters a_0 and z_0. The resolution of the impact parameters is given by the following analytic relation (Appendix A):

$$\sigma = \frac{r_1\sigma_2 \oplus r_2\sigma_1}{r_2 - r_1} \oplus \frac{k_1 r_1}{p_T} = A \oplus \frac{B}{p_T} \tag{3.3.1}$$

The position resolution of the first detector layer at $r = r_1$ is given by σ_1, the position resolution of the second detector layer at $r = r_2$ is given by σ_2. The term $k_1 p_T^{-1}$ describes the rms of the multiple scattering angle at the first plane (3.2.14).

This form can be shown to be an asymptotic solution at very high and very low p_T to the covariances, which are derived from (3.2.20). Hence, the following approximations can be written[13]:

$$\mathrm{cov}(p_a) = A_{aa}^2 + \frac{B_{aa}^2}{p_T^2} \quad \mathrm{cov}(p_a, p_b) = A_{ab}^2 + \frac{B_{ab}^2}{p_T^2} \tag{3.3.2}$$

The terms a and b are indices indicating the track parameters (2.1). The symmetric $5 \otimes 5$ matrix $\boldsymbol{A}$ represents the intrinsic errors on the track parameters and $\boldsymbol{B}$ represents the multiple scattering errors. Both $\boldsymbol{A}$ and $\boldsymbol{B}$ depend on $|\eta|$ but not on p_T. It is important to notice that the expressions for $\boldsymbol{A}$ and $\boldsymbol{B}$, given in (3.3.1), are only valid for the impact parameters. The matrices $\boldsymbol{A}$ and $\boldsymbol{B}$ can be determined via one measurement at low and one at high p_T.

[13] In [1] a different relation is given for the correlation terms: $\rho_{ab} = A_{ab}^2 + B_{ab}^2 / p_T^2$. This relation is not very good and the numerical values given in table 4-3 in [1] are calculated incorrectly and should be ignored.

An arbitrary but useful choice is $p_T = 1$ GeV for the low p_T measurement and $p_T = 1$ TeV for the high p_T measurement. At $p_T = 1$ TeV the influence of the B term is negligible and $\mathrm{cov}(p_a, p_b) = A_{ab}^2$.
In the next sections the data points calculated with `Presol` are compared with this model.

4 Resolutions and correlations

In this chapter the resolutions and correlations of all track parameters are discussed. Firstly the resolutions are discussed as functions of η and p_T. Secondly the correlations are presented.

4.1 Transverse impact parameter resolution

The resolution of the transverse impact parameter as function of p_T is given in figure 4.1.1 ($|\eta| = 0$, ideal field, with and without the B-layer[14]). With the B-layer, the resolution is significantly better, especially for $p_T < 10$ GeV. With the B-layer, the $A \oplus B$ model describes the data very well across the complete p_T range. Without the B-layer, rather big discrepancies of around 20% occur for intermediate p_T values ($1 < p_T < 10$ GeV).

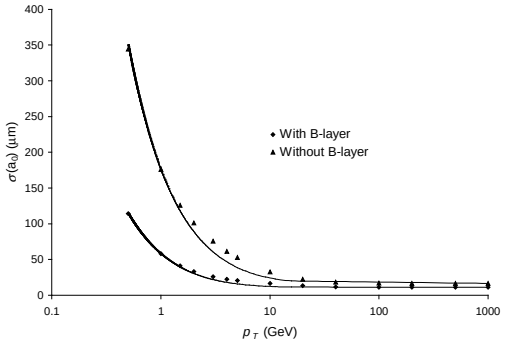

Figure 4.1.1 $\sigma(a_0)$ versus p_T.

$\sigma(a_0)$ as function of $|\eta|$ for $p_T = 1$ TeV and $p_T = 0.5$ GeV is given in figure 4.1.2 and figure 4.1.3. The most important contribution to the resolution comes from the first detector layer[15]. In this case the resolution is nearly constant across the $|\eta|$ coverage of the first detector layer for high p_T tracks. Outside this range the error increases sharply. This behaviour can be seen in figure 4.1.2 (with and without the B-layer[16]). The resolution even improves slightly with increasing $|\eta|$, due to increasing cluster size. For $|\eta| < 2$ the model used for the magnetic field has almost no influence on the results. The degradation without the B-layer for $|\eta| > 2$ however strongly depends on the model used for the magnetic field.

[14] It is not clear if the B-layer will always be present during ATLAS running, especially at high luminosity.

[15] This follows directly from equation (3.3.1), since $r_2 > r_1$

[16] The B-layer extends up to $|\eta| = 2.5$, the first barrel pixel layer only extends up to $|\eta| = 2$.

For low p_T tracks the resolution is almost completely determined by the multiple scattering term and increases with $|\eta|$ (more material). Without the B-layer, the resolution improves again at $|\eta| = 2$ because the end of the coverage of the first pixel barrel layer is reached and the first measurement is now a pixel disk. This is traversed at a more favourable angle than the first barrel layer. It therefore represents less material and the multiple scattering at the first detection reduces[17].

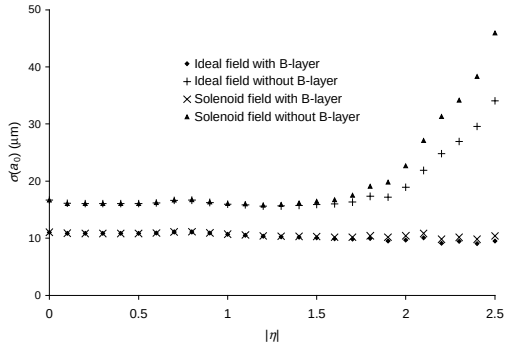

Figure 4.1.2 $\sigma(a_0)$ versus $|\eta|$ for p_T = 1 TeV**.**

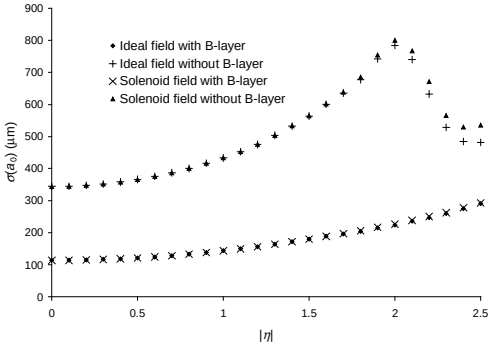

Figure 4.1.3 $\sigma(a_0)$ versus $|\eta|$ for p_T = 0.5 GeV.

4.2 Longitudinal impact parameter resolution

In figure 4.2.1 $\sigma(z_0)$ is given as function of p_T (with and without the B-layer, $|\eta| = 0$). The beam constraint and magnetic field do not influence $\sigma(z_0)$ because the track parameters in the *x*-*y* and *r*-*z* planes are uncorrelated. The $A \oplus B$ model describes the data very well across the complete p_T range, apart from the point at 0.5 GeV.

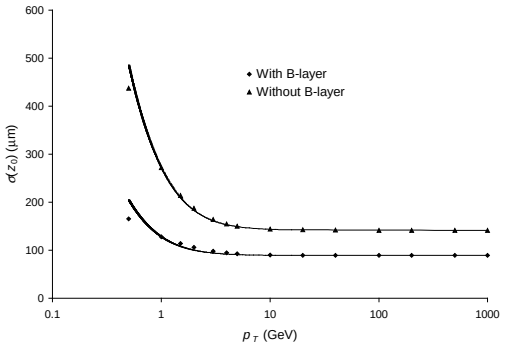

Figure 4.2.1 $\sigma(z_0)$ versus p_T.

[17] Only the multiple scattering at the first measurement layer influences the resolution of the impact parameters.

In figure 4.2.2 and figure 4.2.3, $\sigma(z_0)$ is given as function of $|\eta|$ for $p_T = 1$ TeV and 0.5 GeV respectively. For $p_T = 1$ TeV, $\sigma(z_0)$ is mainly determined by the intrinsic resolution of the first two detector layers and should be approximately constant across the complete $|\eta|$ range covered by these layers ($|\eta| = 2.5$ with the B-layer, $|\eta| = 2$ without the B-layer). In fact the resolution improves slightly at $|\eta| \approx 1$, caused by the increased cluster sizes. For $p_T = 0.5$ GeV, the resolution is determined by the multiple scattering term. In this case, the behaviour is similar to that of the transverse impact parameter. The resolution in the longitudinal direction is significantly worse than in the transverse direction caused by the poorer z resolution of the B-layer and pixel detectors.

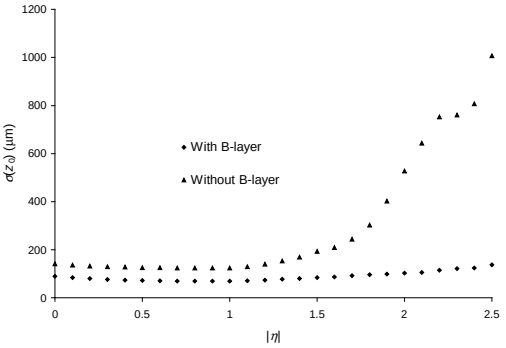

Figure 4.2.2 $\sigma(z_0)$ versus $|\eta|$ for $p_T = 1$ TeV.

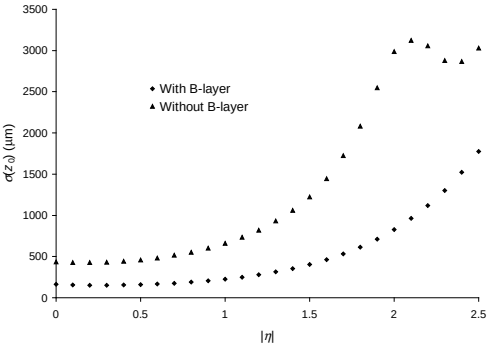

Figure 4.2.3 $\sigma(z_0)$ versus $|\eta|$ $p_T = 0.5$ GeV.

4.3 ϕ –Resolution

In figure 4.3.1 and figure 4.3.2, $\sigma(\phi_0)$ is given as function of p_T ($\eta = 0$, ideal field, with and without the B-layer), without and with beam constraint. Without beam constraint, the $A \oplus B$ model describes the data rather well. With beam constraint, it fails for intermediate p_T values ($1 < p_T < 10$ GeV) and low p_T values ($p_T < 1$ GeV)[18].

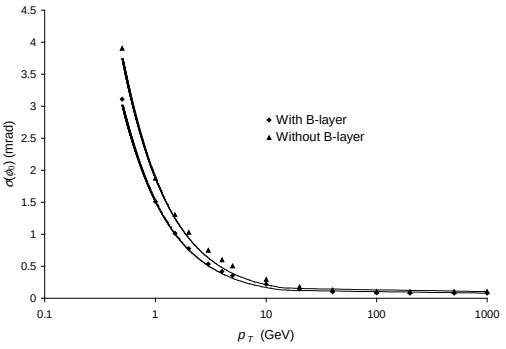

Figure 4.3.1 $\sigma(\phi_0)$ versus p_T, no beam constraint.

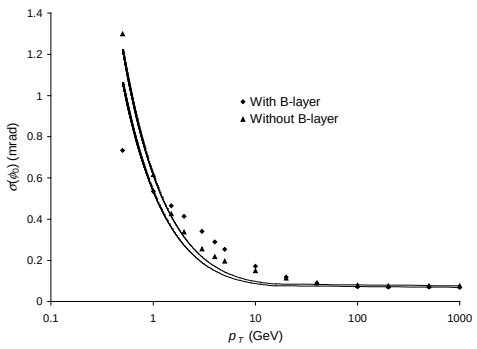

Figure 4.3.2 $\sigma(\phi_0)$ versus p_T, beam constraint.

[18] The $A \oplus B$ model will match at low p_T, if the point at 0.5 GeV instead of 1 GeV is used for determining parameter B. In this case however the discrepancy at intermediate p_T values will be even bigger.

$\sigma(\phi_0)$ as function of $|\eta|$ is given in figure 4.3.3 and figure 4.3.4 for p_T = 1 TeV and p_T = 0.5 GeV (no beam constraint). With the B-layer, the resolution for p_T = 1 TeV is fairly constant in $|\eta|$ and independent of the model for the magnetic field. Without the B-layer, $\sigma(\phi_0)$ increases sharply beyond $|\eta| = 2$. This degradation is strongly influenced by the magnetic field. The behaviour of $\sigma(\phi_0)$ as function of $|\eta|$ for p_T = 0.5 GeV is similar to the behaviour of the impact parameter resolutions.

The corresponding plots with beam constraint are given in figure 4.3.5 and figure 4.3.6. The behaviour is similar to the behaviour with beam constraint. For p_T = 0.5 GeV however, the improvement of the resolution at $|\eta| = 2$ without the B-layer, is much less clear.

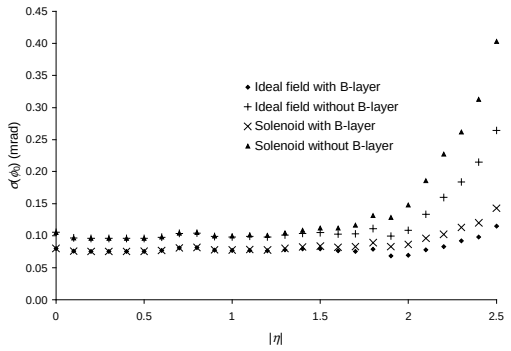

Figure 4.3.3 $\sigma(\phi_0)$ versus $|\eta|$ for p_T = 1 TeV, no beam constraint.

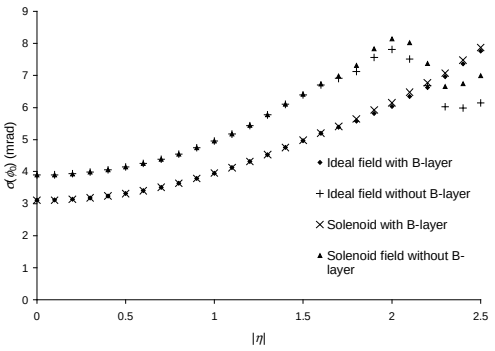

Figure 4.3.4 $\sigma(\phi_0)$ versus $|\eta|$ for p_T = 0.5 GeV, no beam constraint.

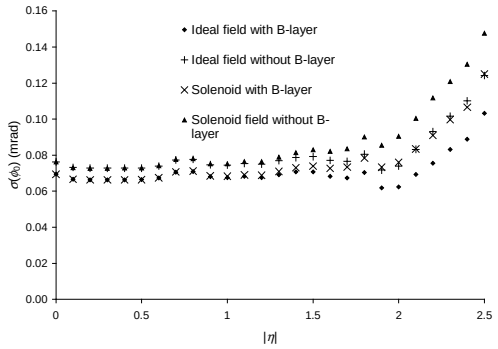

Figure 4.3.5 $\sigma(\phi_0)$ versus $|\eta|$ for p_T = 1 TeV, beam constraint.

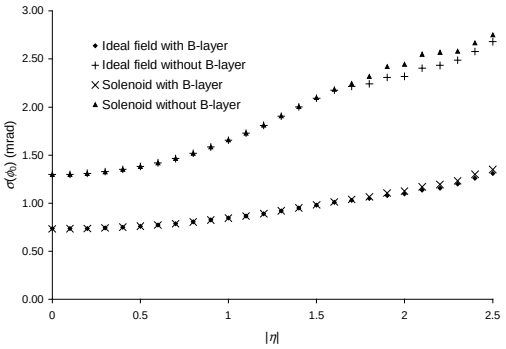

Figure 4.3.6 $\sigma(\phi_0)$ versus $|\eta|$ for p_T = 0.5 GeV, beam constraint.

4.4 cotθ-Resolution

$\sigma(\cot\theta)$ versus p_T is given in figure 4.4.1 ($|\eta| = 0$, with and without B-layer). The $A \oplus B$ model describes the data very well across the complete p_T range. $\sigma(\cot\theta)$ is less sensitive than $\sigma(z_0)$ to the removal of the B-layer.

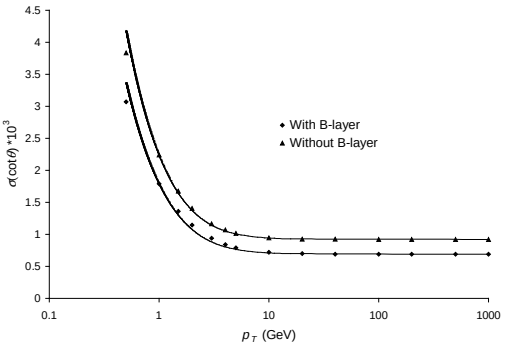

Figure 4.4.1 $\sigma(\cot\theta)$ versus p_T.

$\sigma(\cot\theta)$ versus $|\eta|$ is given in figure 4.4.2 and figure 4.4.3, for $p_T = 1$ TeV and $p_T = 0.5$ GeV. The resolution is almost constant in the barrel area, it increases in the forward area. This behaviour can be explained from (3.2.8) and (3.2.10). These equations show that the z-resolution of the strip detectors is independent of θ in the barrel area and scales with $\cot\theta$ in the endcap area.

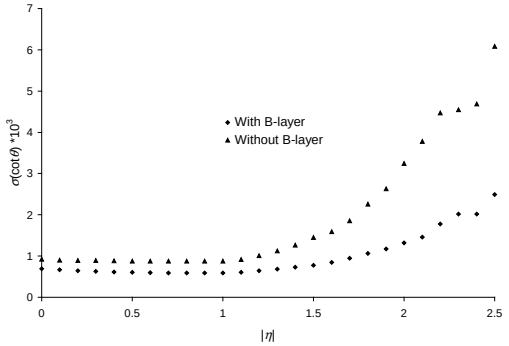

Figure 4.4.2 $\sigma(\cot\theta)$ versus $|\eta|$ for $p_T = 1$ TeV.

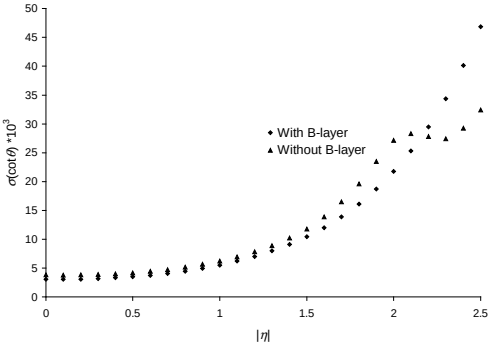

Figure 4.4.3 $\sigma(\cot\theta)$ versus $|\eta|$ for $p_T = 0.5$ GeV.

4.5 Momentum resolution

$\sigma(Q/p_T)$ versus p_T is shown in figure 4.5.1 and figure 4.5.2 ($|\eta| = 0$, ideal field, with and without the B-layer), without and with beam constraint. The $A \oplus B$ model matches the data well, except for $p_T < 1$ GeV.

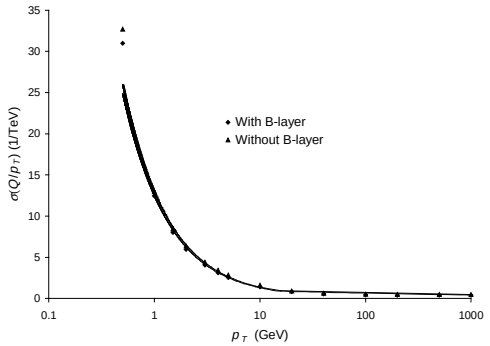

Figure 4.5.1 $\sigma(Q/p_T)$ versus p_T, no beam constraint.

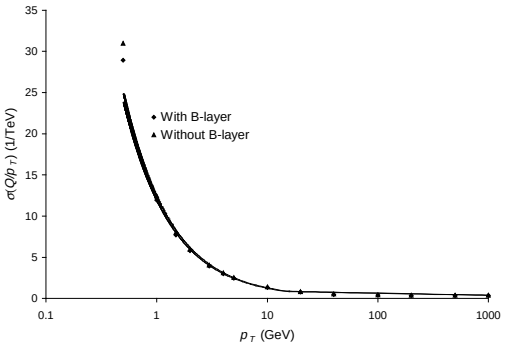

Figure 4.5.2 $\sigma(Q/p_T)$ versus p_T, beam constraint.

$\sigma(Q/p_T)$ versus $|\eta|$ is given in figure 4.5.3 and figure 4.5.4 ($p_T = 1$ TeV and $p_T = 0.5$ GeV, no beam constraint). For $p_T = 1$ TeV, the resolution degrades sharply above $|\eta| = 2$. The B-layer has almost no influence on the resolution in the central part, but beyond $|\eta| = 2$ it helps significantly. Also the field has an important influence above $|\eta| = 2$. For $p_T = 0.5$ GeV the results are almost independent of the use of the B-layer. The magnetic field has some influence above $|\eta| = 2$.

The corresponding plots with beam constraint are given in figure 4.5.5 and figure 4.5.6. Above $|\eta| = 2$, the use of a beam constraint significantly helps to improve the resolution.

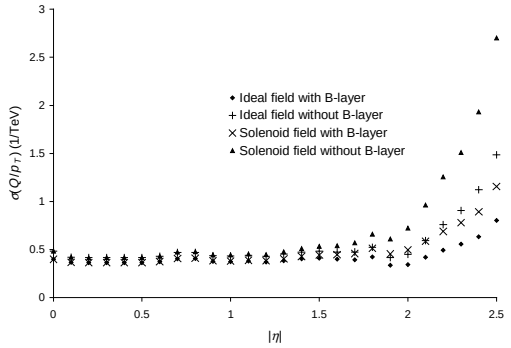

Figure 4.5.3 $\sigma(Q/p_T)$ versus $|\eta|$ for $p_T = 1$ TeV, no beam constraint.

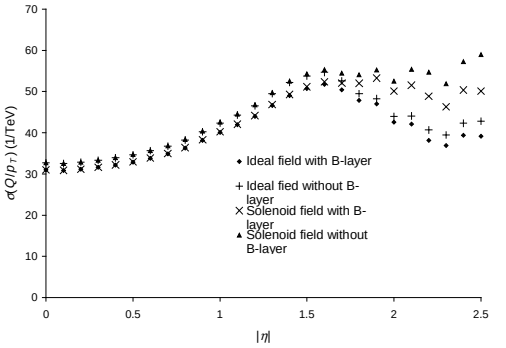

Figure 4.5.4 $\sigma(Q/p_T)$ versus $|\eta|$ for $p_T = 0.5$ GeV, no beam constraint.

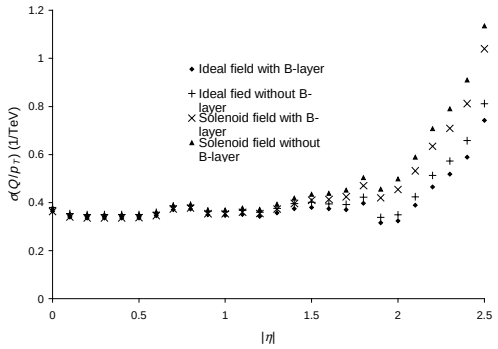

Figure 4.5.5 $\sigma(Q/p_T)$ versus $|\eta|$ for $p_T = 1$ TeV, beam constraint.

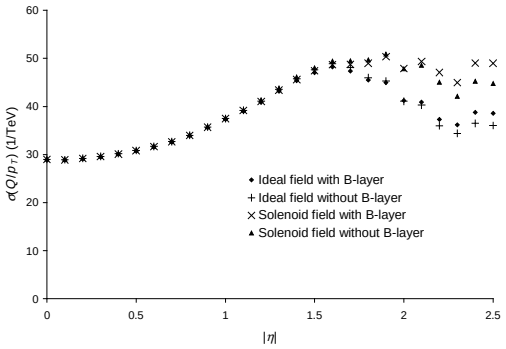

Figure 4.5.6 $\sigma(Q/p_T)$ versus $|\eta|$ for $p_T = 0.5$ GeV, beam constraint.

4.6 Correlations

The covariances cov(a_0, ϕ_0), cov(a_0, Q/p_T), cov(z_0, cotθ), cov(ϕ_0, Q/p_T) and the corresponding normalised correlations, are given as function of p_T in figure 4.6.1 to figure 4.6.10. For all covariances, the $A \oplus B$ model matches the data very well, except for $p_T < 1$ GeV. In the case of beam constraint measurements of cov(ϕ_0, Q/p_T), the $A \oplus B$ model describes the data less well. Using the B-layer always significantly reduces the magnitude of all correlation coefficients.

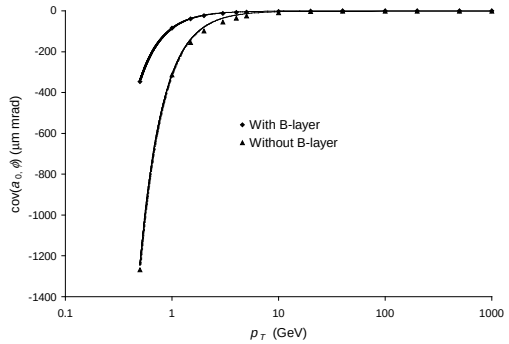

Figure 4.6.1 cov(a_0, ϕ_0) versus p_T.

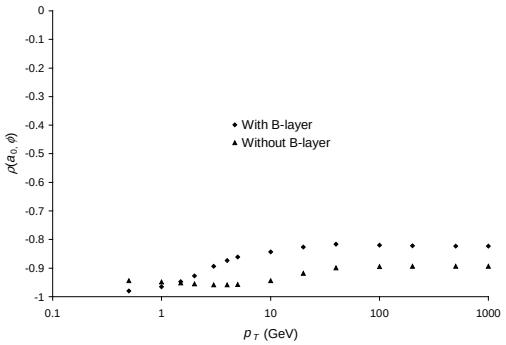

Figure 4.6.2 $\rho(a_0, \phi_0)$ versus p_T.

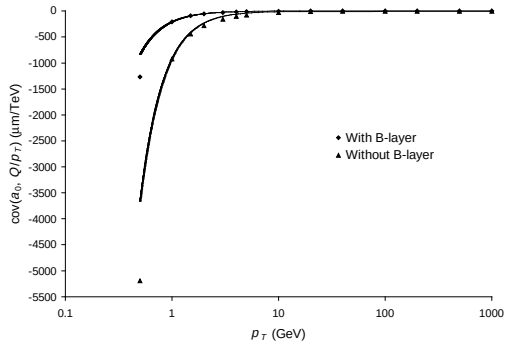

Figure 4.6.3 cov(a_0, Q/p_T) versus p_T.

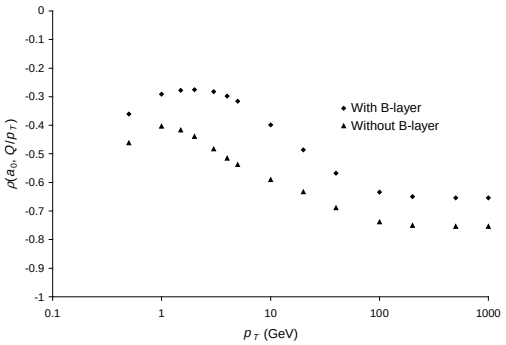

Figure 4.6.4 $\rho(a_0, Q/p_T)$ versus p_T.

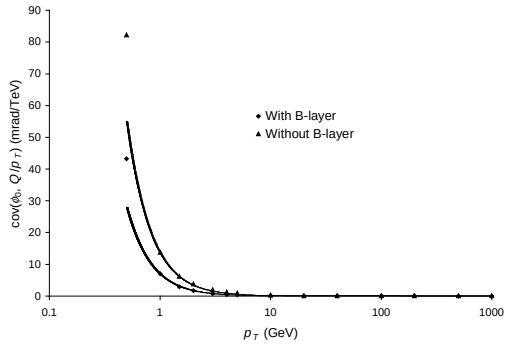

Figure 4.6.5 cov(ϕ_0, Q/p_T) versus p_T, no beam constraint.

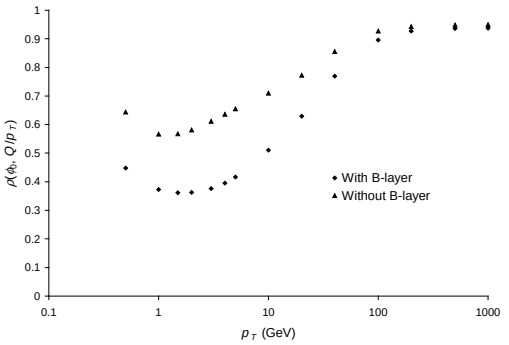

Figure 4.6.6 $\rho(\phi_0, Q/p_T)$ versus p_T, no beam constraint.

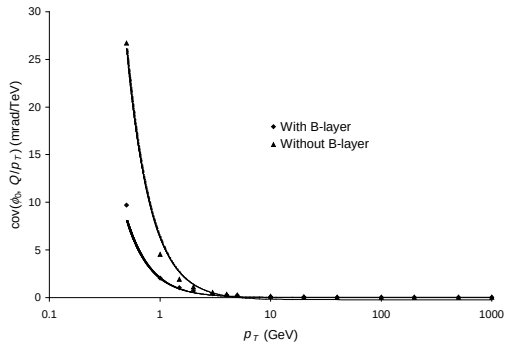

Figure 4.6.7 cov(ϕ_0, Q/p_T) versus p_T, beam constraint.

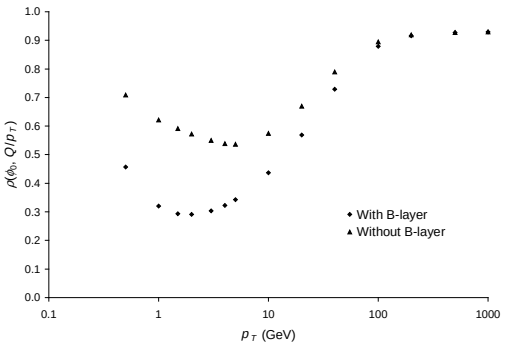

Figure 4.6.8 $\rho(\phi_0, Q/p_T)$ versus p_T, beam constraint.

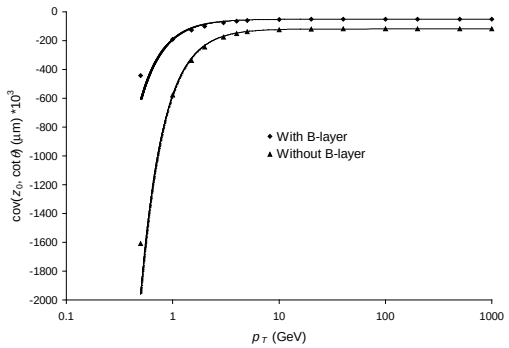

Figure 4.6.9 cov(z_0, cotθ) versus p_T.

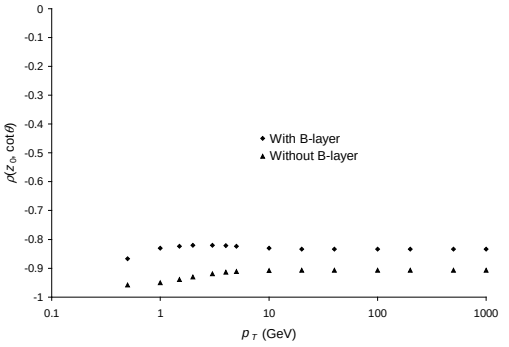

Figure 4.6.10 $\rho(z_0, \cot\theta)$ versus p_T.

4.7 Conclusions

From the above data can be concluded that the $A \oplus B$ model does not always matches the data across the complete p_T range. Since all elements of the covariance matrix vary smoothly with η and p_T, it is more suitable to represent them by interpolating between matrices calculated at selected η and p_T values. The $A \oplus B$ model is only used for the interpolation. The amount of data needed to describe all track parameter resolutions and tails for the Inner Detector for all particle types is around 150 kB. Keeping this constantly in memory is not a problem for typical HEP computing platforms. The influence of the non uniformity of the magnetic field is significant for the track parameters in the *x*-*y* plane at high $|\eta|$ (above $|\eta| \sim 1.5$ or ~ 2, depending on which parameter is

being considered). The use of a solenoid field description will give more realistic results, which will be important for some physics studies.

5 Software Description

5.1 Subroutine Overview

All routines have been written in FORTAN 77 and have been developed on HP-UX-9.x as well as Windows NT 4.0 systems. All floating point calculations have been implemented in double precision. The software can be found on the following afs location:

```
/afs/cern.ch/user/r/reichold/public/my_atlfast
```

In this location also a copy of this document is kept in postscript and Word97 format. A list of all FORTRAN files with a short description of their functionality is given in table 1.

Table 1 Overview of files and routines

File	Subroutine (S) / Function (F)	Description
`Id_init_resol.f`	`Id_init_resol` (S)	read resolution data from file
`Id_init_tail.f`	`Id_init_tail` (S)	read tail from file (dummy)
`Id_interpol_resol.f`	`Id_interpol_resol` (S)	calculate covariance matrix for given η and p_T
`Id_smear.f`	`Id_smear` (S)	smear vector of track parameters with covariance matrix
`Id_xxx_resol.f`	`Id_resol` (S)	main routine. Called by the user.
`dcorgen.f`	`dcorgen` (S)	double precision random number generator
`dcorset.f`	`dcorset` (S)	
`drnorml.f`	`drnorml` (S)	calculate vector of double precision correlated random numbers
`make_eta.f`	`make_eta` (F)	double precision $\theta \rightarrow \eta$
	`make_theta` (F)	double precision $\eta \rightarrow \theta$
	`cot` (F)	double precision cotangens
	`acot` (F)	double precision acotangens

The main user callable routine is `Id_resol`. All other routines are internal to the package and should not be called by the user.The calling sequence and physical units of `Id_resol` can be found in section 5.3.

5.2 Data file overview

The files containing the resolution data are named `id_resol_particle_XYZ.dat` or `id_tail_particle_XYZ.dat`. The fields `resol` and `tail` indicate that the data describes either the Gaussian part or the tail of the distributions[19]. The field `particle` describes the particle type (`el` = electron, `mu` = muon and `pi` = pion). The field `X` describes the detector geometry configuration. Currently two options are possible:

`X` = 0: with the B-layer

`X` = 1: without the B-layer

The field `Y` describes the model used for the magnetic field. Currently two options are possible:

`Y` = 0: approximated real solenoid field

`Y` = 1: ideal homogeneous 2T field

The field `Z` indicates if a beam constraints is used or not:

`Z` = 0: data with beam constraint

`Z` = 1: data without beam constraint

A fraction of the data file `id_resol_mu_011.dat` is shown below. First the η and then the p_T base points are given. Both must be in ascending order. There must not be more than `n_pt_max` p_T base points and `n_eta_max` η base points. Both `n_pt_max` and `n_eta_max` are currently set to 100. Following this, for each base point combination first a row of 5 sigmas and then a row of 4 correlation coefficients are given. The p_T base point varies first and the η base point second. At the end of the file summarising comments on the detector geometry, the field, the beam constraint and the authorship are appended. The units used in this file are a_0 [μm], z_0 [μm], ϕ [mrad], cot(θ) [1/1000] and $\%/p_T$ [TeV^{-1}] These units differ from the units used for calling `Id_resol`, in order to be able to compare the results more easily to [1].

[19] The tails are not yet used.

```
number of eta-bins
26
vector of eta_bins
.000D+00 .100D+00 .200D+00 .300D+00 .400D+00
.500D+00 .600D+00 .700D+00 .800D+00 .900D+00
.100D+01 .110D+01 .120D+01 .130D+01 .140D+01
.150D+01 .160D+01 .170D+01 .180D+01 .190D+01
.200D+01 .210D+01 .220D+01 .230D+01 .240D+01
.250D+01
number of pt-bins
14
vector of pt_bins
.500D+00 .100D+01 .150D+01 .200D+01 .300D+01
.400D+01 .500D+01 .100D+02 .200D+02 .400D+02
.100D+03 .200D+03 .500D+03 .100D+04
parameter order A0, Z0, phi0, cotan(Theta) char/Pt
parameter order 1/pt-phi 1/pt-A0 phi-A0 cot(theta)-z0
 .11394D+03  .16562D+03  .31086D+01  .30735D+01  .30987D+02
 .44819D+00 -.36065D+00 -.98010D+00 -.86688D+00
 .58099D+02  .12810D+03  .15110D+01  .17886D+01  .12434D+02
 .37295D+00 -.29190D+00 -.96588D+00 -.83041D+00
                .
                .
          (for all p_T and η combinations)
                .
                .
.95368D+01  .13712D+03  .11510D+00  .24932D+01  .80379D+00
 .96883D+00 -.71476D+00 -.82514D+00 -.84563D+00
who made this : Reinier Dankers, with presol.f
when was it made : 06.10.1997
data origin : TDR, direct averages of covariance matrix
fields : ideal 2T solenoid field
vertex constraint : no constraint
B-layer : including B-layer
```

5.3 Subroutines

Id_resol

A list of parameters of this subroutine is given below:

`part_type`	integer	input	particle type (`Pythia` convention)
`id_config`	integer	input	detector geometry, magnetic field and track constraint configuration (see section 5.2)
`to_be_smeared`	double[5]	input	incoming track
`smeared`	double[5]	output	smeared track
`sigma`	double[5][5]	output	covariance matrix

This subroutine is the main routine of the package. It is the only routine that should be called directly by the user. On the first call it automatically initialises the data structures for all particle types carrying the covariance

matrices and tails. The initialisation is done for one detector configuration only. A request for a different configuration in the same run is ignored. The data structures for the tails are already created but no initialisation is done yet. The track that is to be smeared should be given in `to_be_smeared` with the track parameters in the order and units according to the ATLAS convention:

a_0 [cm], z_0 [cm], ϕ [rad, $0 < \phi < 2\pi$], cot(θ) [1], $\%/_{p_T}$ [GeV^{-1}]

The smeared track is returned in `smeared`. There is no information returned about the tail yet. The covariance matrix belonging to the smeared track is returned in `sigma`. If an uncharged particle is passed to the routine it stops and prints an error message.

Id_interpol_resol

A list of parameters of the subroutine is given below:

`n_pt_max`	integer	input	dimension of `pt` and p_T dimension of `resol_par`
`pt`	double[`n_pt_max`]	input	p_T base points
`n_eta_max`	integer	input	dimension of `eta` and η dimension of `resol_par`
`eta`	double[`n_eta_max`]	input	η base points
`resol_par`	double[9, `n_eta_max`, `n_pt_max`]	input	relevant covariances for each η and p_T base point
`n_pt_used`	integer	input	number of `pt` base points used
`n_eta_used`	integer	input	number of `eta` base points used
`pt0`	double	input	p_T value to be interpolated to
`eta0`	double	input	η value to be interpolated to
`sigma`	double[5][5]	output	interpolated covariance matrix at `pt0` and `eta0`
`warningId`	integer	output	warning flag, 0 = success, 1 = `pt0` or `eta0` in edge of calibrated range

`Id_interpol_resol` calculates the covariance matrix for a given p_T and η value by two dimensionally interpolating between covariances given in `resol_par` for the nearest base points. If the requested p_T and η are in an edge bin of `resol_par`, a warning flag is set. If they are outside of the range described in `resol_par`, the subroutine prints and error message and stops. The interpolation is linear in p_T^{-2} and η (3.3.2).

Id_smear

A list of parameters of the subroutine is given below:

`to_be_smeared`	double[5]	input	unsmeared track
`sigma`	double[5][5]	input	covariance matrix of Gaussian part
`tail`	double[5][5]	input	covariance matrix of tail (currently dummy)
`tail_type`	integer	input	tail type (0 = no tail)
`smeared`	double[5]	output	smeared track

This subroutine smears the 5 parameters of `to_be_smeared` according to the covariance matrix sigma using a set of 5 correlated double precision random numbers created by `drnorml`, which internally uses `dcorgen` and `dcorset`. These routines are double precision version of the CERN library routines `rnorml`, `corgen` and `corset`. If a tail is requested for smearing the current version prints an error message and stops because there is no data available for tails yet.

Id_init_resol

A list of parameters of the subroutine is given below:

`fname`	char*	input	name of data file
`n_eta_max`	integer	input	dimension of `eta_array` and η dimension of `resol_par`
`eta_array`	double[`n_eta_max`]	output	η base points
`n_pt_max`	integer	input	dimension of `pt_array` and p_T dimension of `resol_par`
`pt_array`	double[`n_pt_max`]	output	p_T base points
`resol_par`	double[9, `n_eta_max`, `n_pt_max`]	output	relevant covariances for each η and p_T base point
`n_eta_used`	integer	output	number of η base points used
`n_pt_used`	integer	output	number of p_T base points used

This subroutine fills the 9 relevant elements of the covariance matrix into `resol_par` with data from a file specified by `fname`. It returns the filled `resol_par` and information about how many base points were used to fill it. It also returns the base points themselves in the arrays `pt_array` and `eta_array`. Several checks are done on the data:

- The number of η and p_T base points must not exceed the maximum of `n_eta_max` and `n_pt_max`.
- The base points must be in strictly ascending order.
- The sigmas must be positive.
- The correlation terms must be in the allowed range: $|\rho| \leq 1$.
- For all base point pairs, the covariance matrices are calculated and checked for positive definiteness using the CERN library routine `DSFAC`.

If any of the above checks fail, the routine prints the reason and stops. The routine also prints its results to standard output.

6 Future Plans

The four main steps in the future development of this package are given below.

1. **Tails for muons and pions**

   This activity awaits input data from other collaborators in the Inner Detector performance group. Necessary is a description of the tails as function of η and p_T. The package is well prepared for the use of tails, provided they are independent from the Gaussian centres.

2. **Electrons**

   It is not yet clear how the resolutions for electrons are best described because electrons continuously loose energy through Bremsstrahlung. Therefore electron resolutions are not simple Gaussian centres with tails as those for muons and pions. The question of how to describe these resolutions will be answered within the Inner Detector performance group in the next few months.

3. **Other performance variables**

   Besides the track parameter resolutions there are other variables which characterise the performance of the Inner Detector. Some of these are the tracking efficiency, the transition radiation efficiency and the probability for identifying V^0s, such as K_s, in the Inner Detector. The tracking efficiency is the most straight forward of these parameters. The possibility to parameterise the tracking efficiency is currently investigated using full detector simulations.

4. Migration to an object oriented C++ version

An object oriented C++ version of the package is currently begin developed. The FORTRAN code is written with this aim in mind and avoids the use of common blocks completely to ease the transition to C++. The current level of independence from the framework of ATLFAST will be maintained but some base classes such as tracks and covariance matrices will most likely have to be shared across the whole of ATLFAST C++.

7 Acknowledgements

We wish to explicitly acknowledge that the results for the Inner Detector resolutions were obtained with a modified version of the program Presol. This program has been developed over several years by Alan Poppleton with contributions from many others. We would furthermore like to thank Elzbieta Richter-Was for helping with the interface to ATLFAST and her efforts to include the package as part of the official ATLFAST program. For numerous discussions and good advice we would like to thank Bob van Eijk.

8 References

1. ATLAS Inner Detector community: Inner Detector technical design report (volume 1), ATLAS TDR4, CERN/LHCC97-16, April 1997.
2. S.J. Haywood: Impact parameter resolution in the presence of multiple-scattering, ATLAS INDET-NO-091, January 1995.
3. S.J. Haywood : Helix fits with stereo measurements, ATLAS INDET-NO-095, January 1995
4. A. Poppleton: private communication.
5. E. Richter-Was, D. Froidevaux and L. Poggioli: ATLFAST 1.0, a package for particle level analysis, ATLAS PHYS-NO-079, March 96.
6. Particle data group: Particle Physics Booklet, July 1996.
7. V.I. Klyukhin, A. Poppleton, J. Schmitz: Field integrals for the ATLAS tracking volume, ATLAS INDET-NO-23, February 1993.

Appendix A. The resolution of the impact parameters in the case of two detector layers

In general for any $n \otimes n$ matrix $\boldsymbol{M}$ given by:

$$\boldsymbol{M} = \begin{pmatrix} M_{11} & M_{12} & \cdots & M_{1n} \\ M_{21} & M_{22} & \cdots & M_{2n} \\ \vdots & \vdots & \vdots & \vdots \\ M_{n1} & M_{n2} & \cdots & M_{nn} \end{pmatrix} \tag{A.1}$$

If $\boldsymbol{M}$ is not singular one can find the inverse matrix $\boldsymbol{K} = \boldsymbol{M}^{-1}$ as:

$$\boldsymbol{K} = \frac{1}{\det \boldsymbol{M}} \begin{pmatrix} K_{11} & K_{12} & \cdots & K_{1n} \\ K_{21} & K_{22} & \cdots & K_{2n} \\ \vdots & \vdots & \vdots & \vdots \\ K_{n1} & K_{n2} & \cdots & K_{nn} \end{pmatrix} \tag{A.2}$$

The term K_{jk} is the cofactor or adjunct determinant of M_{jk} in det$\boldsymbol{M}$.

If the r-ϕ and r-z plane are treated separately, the $(5 + 2n) \otimes (5 + 2n)$ matrix $\boldsymbol{C}^{-1}$ mentioned in (3.2.20) can be split into a matrix $\boldsymbol{C}_{r\phi}^{-1}$ of dimension $(3 + n) \otimes (3 + n)$ and a matrix $\boldsymbol{C}_{rz}^{-1}$ of dimension $(2 + n) \otimes (2 + n)$. From equation (3.2.20) follows that, in the case of two detector planes, $\boldsymbol{C}_{rz}^{-1}$ is given by:[20]

$$\boldsymbol{C}_{rz}^{-1} = \begin{pmatrix} 1 & 0 \\ r_1 & 0 \\ 0 & 1 \\ 0 & 0 \end{pmatrix} \begin{pmatrix} w_1^2 & 0 \\ 0 & \lambda_1^2 p_T^2 \end{pmatrix} \begin{pmatrix} 1 & r_1 & 0 & 0 \\ 0 & 0 & 1 & 0 \end{pmatrix} + \begin{pmatrix} 1 & 0 \\ r_2 & 0 \\ r_2 - r_1 & 0 \\ 0 & 1 \end{pmatrix} \begin{pmatrix} w_2^2 & 0 \\ 0 & \lambda_2^2 p_T^2 \end{pmatrix} \begin{pmatrix} 1 & r_2 & r_2 - r_1 & 0 \\ 0 & 0 & 0 & 1 \end{pmatrix} \tag{A.3}$$

with $w_i = 1/\sigma_{i,z}$, and $\lambda_i = k_{i,2}^{-2}$ (3.2.14). Performing the matrix multiplication gives:

$$\boldsymbol{C}_{rz}^{-1} = \begin{pmatrix} w_1^2 + w_2^2 & w_1^2 r_1 + w_2^2 r_2 & w_2^2 (r_2 - r_1) & 0 \\ w_1^2 r_1 + w_2^2 r_2 & w_1^2 r_1^2 + w_2^2 r_2^2 & w_2^2 r_2 (r_2 - r_1) & 0 \\ w_2^2 (r_2 - r_1) & w_2^2 r_2 (r_2 - r_1) & w_2^2 (r_2 - r_1)^2 + \lambda_1^2 p_T^2 & 0 \\ 0 & 0 & 0 & \lambda_2^2 p_T^2 \end{pmatrix} \tag{A.4}$$

The determinant of this matrix is given by:

$$\det \boldsymbol{C}_{rz}^{-1} = \lambda_1^2 p_T^2 w_1^2 \lambda_2^2 p_T^2 w_2^2 (r_2 - r_1)^2 \tag{A.5}$$

From equation (A.2) follows:

$$\mathrm{cov}(z_0) = C_{rz,11} = \frac{\begin{vmatrix} w_1^2 r_1^2 + w_2^2 r_2^2 & w_2^2 r_2 (r_2 - r_1) \\ w_2^2 r_2 (r_2 - r_1) & w_2^2 (r_2 - r_1)^2 + \lambda_1^2 p_T^2 \end{vmatrix}}{\lambda_1^2 p_T^2 w_1^2 w_2^2 (r_2 - r_1)^2} \tag{A.6}$$

After some manipulation one finally gets:

$$\mathrm{cov}(z_0) = \frac{r_1^2}{\lambda_1^2 p_T^2} + \frac{\frac{r_1^2}{w_2^2} + \frac{r_2^2}{w_1^2}}{(r_2 - r_1)^2} = \frac{k_{1,2}^2 r_1^2}{p_T^2} + \frac{r_1^2 \sigma_{2,z}^2 + r_2^2 \sigma_{1,z}^2}{(r_2 - r_1)^2} \tag{A.7}$$

One can deduce a similar expression for $\mathrm{cov}(a_0)$. The Q/p_T term should be ignored in this case, because Q/p_T can not be measured with only two planes.

[20] To calculate $\boldsymbol{C}_{rz}^{-1}$, also the vectors $\boldsymbol{p}$ and $\boldsymbol{p}_{ms}$ and the matrices $\boldsymbol{V}_i$ and $\boldsymbol{D}_i$ need to be split into two uncorrelated parts; one in the r-ϕ plane and another in the r-z plane.